Author(s): Palomäki, Tommi; Wester, Niklas; Johansson, Leena-Sisko; Laitinen, Mikko; Jiang, Hua; Arstila, Kai; Sajavaara, Timo; Han, Jeon G.; Koskinen, Jari; Laurila, Tomi

Title: Characterization and Electrochemical Properties of Oxygenated Amorphous Carbon (a-C) Films

Year: 2016

Version:

Please cite the original version:

Palomäki, T., Wester, N., Johansson, L.-S., Laitinen, M., Jiang, H., Arstila, K., Sajavaara, T., Han, J. G., Koskinen, J., & Laurila, T. (2016). Characterization and Electrochemical Properties of Oxygenated Amorphous Carbon (a-C) Films. Electrochimica Acta, 220, 137-145. https://doi.org/10.1016/j.electacta.2016.10.063

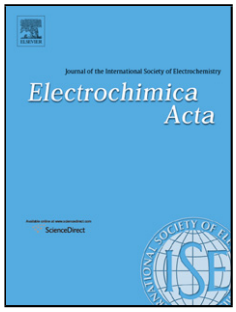

Title: Characterization and Electrochemical Properties of Oxygenated Amorphous Carbon (a-C) Films

Author: Tommi Palomäki Niklas Wester Leena-Sisko Johansson Mikko Laitinen Hua Jiang Kai Arstila Timo Sajavaara Jeon G. Han Jari Koskinen Tomi Laurila

PII: S0013-4686(16)32150-8
DOI: http://dx.doi.org/doi:10.1016/j.electacta.2016.10.063
Reference: EA 28151

To appear in: *Electrochimica Acta*

Received date: 31-7-2016
Revised date: 10-10-2016
Accepted date: 10-10-2016

Please cite this article as: Tommi Palomäki, Niklas Wester, Leena-Sisko Johansson, Mikko Laitinen, Hua Jiang, Kai Arstila, Timo Sajavaara, Jeon G.Han, Jari Koskinen, Tomi Laurila, Characterization and Electrochemical Properties of Oxygenated Amorphous Carbon (a-C) Films, Electrochimica Acta http://dx.doi.org/10.1016/j.electacta.2016.10.063

Characterization and Electrochemical Properties of Oxygenated Amorphous Carbon (a-C) Films

Tommi Palomäki[a], Niklas Wester[b], Leena-Sisko Johansson[c], Mikko Laitinen[d], Hua Jiang[e], Kai Arstila[d], Timo Sajavaara[d], Jeon G. Han[e], Jari Koskinen[b] and Tomi Laurila[a*]

[a]Department of Electrical Engineering and Automation, School of Electrical Engineering, Aalto University, Espoo, Finland

[b]Department of Materials Science and Engineering, School of Chemical Technology, Aalto University, Espoo, Finland

[c]Department of Forest Products Technology, School of Chemical Technology, Aalto University, Espoo, Finland

[d]Department of Physics, University of Jyvaskyla, Jyväskylä, Finland

[e]Department of Applied Physics, School of Science, Aalto University, Espoo, Finland

[e]Center for Advanced Plasma Surface Technology, Sungkyunkwan University, Suwon, South Korea

*Corresponding author: T. Laurila

E-mail: tomi.laurila@aalto.fi. Telephone: +358 503414375

Abstract

Amorphous carbon (a-C) films with varying oxygen content were deposited by closed-field unbalanced magnetron sputtering with the aim to understand the effect of oxygen on the structural and physical properties of the films and subsequently correlate these changes with electrochemical properties. The a-C films were characterized by transmission electron microscopy, helium ion microscopy, atomic force microscopy, Raman spectroscopy, X-ray photoelectron spectroscopy and time-of-flight elastic recoil detection analysis. The electrochemical properties were studied by electrochemical impedance spectroscopy and cyclic voltammetry with several redox systems ($Ru(NH_3)_6^{2+/3+}$, $Fe(CN)_6^{3-/4-}$, dopamine and ascorbic acid). The results indicated that the carbon films are amorphous with an I_D/I_G ratio near 2.6. The oxygen content of the films seemed to saturate at around 11 at. %, whereas the amount of surface oxygen functional groups increased steadily with increasing oxygen inflow during deposition. O/C ratio increased from 0.09 to 0.19. A significant increase in film resistivity was observed with increasing oxygen content. Lightly oxygenated a-C films showed a low charge transfer resistance (R_{ct}) and reversible electron transfer for $Ru(NH_3)_6^{2+/3+}$ whereas both R_{ct} and ΔE_p increased considerably for heavily oxygenated films. The inner sphere redox systems were significantly affected by the surface oxygen functional groups with dopamine and ascorbic acid showing a linear increase in ΔE_p and E_{pa}, respectively, with increasing oxygen content. $Fe(CN)_6^{3-/4-}$ did not show a clear trend but was still clearly affected by the increase in oxygen content. The double layer capacitance was about 1 $\mu F/cm^2$ for all the oxygenated a-C films.

Keywords: oxygenated amorphous carbon, electron transfer, cyclic voltammetry, electrochemical impedance spectroscopy, unbalanced magnetron sputtering

1. Introduction

Carbon based electrodes have been extensively used in electrochemical analysis due to their wide potential window, low background current and the large extent to which their structure and surface chemistry can be modified. Carbon films deposited by unbalanced magnetron sputtering (UBMS) have recently attracted attention because their structure, such as sp^2/sp^3 ratio and crystallinity, can be extensively modified by varying for example ion irradiation energy, bias voltage or substrate temperature [1,2]. In addition, reactive gases such as nitrogen [3], oxygen [4,5] or hydrogen [6] can be introduced in the deposition chamber during sputtering to dope and modify the carbon films. These changes in film structure and chemistry lead to markedly different electrochemical properties [6-8]. The incorporation of nitrogen and hydrogen into carbon films has been more thoroughly researched than that of oxygen from a structural and physical point of view. Furthermore, although the role of surface oxygen functional groups on carbon materials has been widely studied [9], there is still much to be investigated to understand their role in the oxidation of several inner sphere redox systems such as dopamine and ascorbic acid.

In this work, we have deposited amorphous carbon (a-C) films with a varying oxygen content by closed-field unbalanced magnetron sputtering (CFUBMS). The aim was to correlate the changes in physical structure and surface chemistry with the electrochemical properties. The a-C films were characterized by transmission electron microscopy (TEM), helium ion microscopy (HIM), atomic force microscopy (AFM), Raman spectroscopy, X-ray photoelectron spectroscopy (XPS) and time-of-flight elastic recoil detection analysis (ToF-ERDA). The electrochemical properties were studied by electrochemical impedance spectroscopy and cyclic voltammetry with several redox probes encompassing both outer ($Ru(NH_3)_6^{2+/3+}$) and inner ($Fe(CN)_6^{3-/4-}$, dopamine, ascorbic acid) sphere systems.

2. Experimental

2.1. Deposition

The carbon films were deposited on boron-doped Si (100) by closed-field unbalanced magnetron sputtering (CFUBMS) in pulsed DC mode. The target was a 4-inch graphite disk (99.99% purity) and the deposition was carried out at room temperature. The DC power was 2000 W and the frequency 100 kHz at a fixed working pressure of 3 mTorr during deposition. Argon gas flow inside the deposition chamber was controlled with a mass flow controller and kept constant at 80 sccm. The inflow of oxygen was varied between 2 and 14 sccm to obtain a series of carbon films with an increasing amount of oxygen. A reference sample (labeled Ref) with only Ar gas was made for comparison. Samples are named according to the inflow of oxygen during deposition (2, 6, 10, 12 or 14 sccm). The thickness of the films varied between roughly 190 nm (ref) and 155 nm (O14).

2.2. Transmission electron microscopy (TEM)

Transmission electron microscopy was used to investigate the microstructure of the a-C films with a JEM-2200 FS microscope (JEOL) equipped with an EDS. The TEM was operated at 200 kV. Cross-sectional TEM samples were prepared by focused ion beam (FIB) by using first 30 kV for thinning and subsequently 5 kV for final polishing. Polymer ink was used as the filler material with 70-80 nm of sputtered Pt and FIB deposited Pt-C to protect the a-C films during thinning.

2.3. Helium-ion microscopy (HIM)

Surface morphology of the a-C films was studied with a Zeiss Orion Nanofab helium-ion microscope at the Nanoscience Center of the University of Jyvaskyla. No additional coatings were applied before imaging.

2.4. Atomic force microscopy (AFM)

Atomic force microscopy was carried out to measure the roughness of the a-C films using a DI3100 AFM (Veeco Instruments). The instrument was operated in tapping mode with a Tap150AI-G silicon AFM probe (Budget Sensors). Average roughness (R_a) was calculated from three 2 µm x 2 µm areas on each sample. NanoScope v6.13R1 was used for surface roughness analysis.

An Ntegra Aura scanning probe microscope (NT-MDT) was used for conductive AFM measurements in contact mode with conductive CSG30/Pt probes (Golden Silicon Probes). The average current flowing through the studied film area (5 µm x 5 µm) was obtained under an applied probe voltage of 0.5 V.

2.5. Raman spectroscopy

Visible Raman spectroscopy (LabRAM HR, Jobin Yvon Horiba) was used to study the bonding configuration of the a-C films. The system was equipped with an argon laser (wavelength of 514 nm, power 10 mW) and BX41 (Olympus) microscope and 100x objective lens with a spot size of less than 1 µm. The Raman spectra were fitted with a double Gaussian function and the I_D/I_G ratio was obtained from the area ratio of the peaks.

2.6. X-ray photoelectron spectroscopy (XPS)

Surface chemistry of the a-C films was evaluated with X-ray photoelectron spectroscopy (AXIS Ultra, Kratos Analytical), using monochromatic Al Kα irradiation at 100 W under neutralization. Samples were pre-evacuated overnight. Wide range surveys and high-resolution spectra of C 1s and O 1s regions were recorded in triplicate, with an analysis area of less than 1 mm^2. A fresh piece of 100 % cellulose filter paper (Whatman) was measured with each sample batch as an in-situ reference [10]. The data was analyzed using CasaXPS. The binding energies were charge-corrected with the help of the cellulose reference using 286.7 eV for carbon atoms which are singly bonded to one oxygen atom [11].

2.7. Time-of-flight elastic recoil detection analysis (ToF-ERDA)

Elemental depth profiles of the a-C films were measured using a time-of-flight recoil detection analysis system. A detailed description of the method and apparatus can be found in [12]. The ion beam was a 13.6 MeV ^{79}Br from the 1.7 MV Pelletron accelerator at the Accelerator Laboratory of the University of Jyvaskyla. Tilt angle was 20 degrees relative to the ion beam direction. Data was analyzed using Potku software [13].

2.8. Electrochemical impedance spectroscopy (EIS)

Electrochemical impedance spectroscopy measurements were made with a Gamry Reference 600 potentiostat with the same cell and electrode setup as in cyclic voltammetry (see below). The AC signal amplitude was 15 mV, the frequency range from 0.1 Hz to 150 kHz, the DC bias was set at the formal potential of the $Ru(NH_3)_6^{3+/2}$ redox couple as determined by CV (around -0.165 V vs Ag/AgCl). The solution used was 5 mM $Ru(NH_3)_6^{3+/2}$ in 1 M KCl.

The EIS data was fitted with a Randles circuit model with a solution resistance (R_s) in series with a parallel circuit composed of a charge transfer resistance (R_{ct}), a Warburg element (W) and a constant phase element (CPE) replacing the double-layer capacitance (C_{dl}). The standard heterogeneous rate constant (k^0) was obtained from the following equation:

$$k^0 = \frac{\mathrm{RT}}{F^2 A R_{ct} (c_O^b)^{\alpha} (c_R^b)^{1-\alpha}} \quad (1)$$

where R is the gas constant, T the temperature, F the Faraday constant, A the geometrical area of the electrode, c the concentration of $Ru(NH_3)_6^{3+/2}$ and α the transfer coefficient (a value of 0.5 was used). The subscripts O and R denote the oxidized and reduced species, respectively, and the superscript b denotes the bulk concentration.

2.9. Cyclic voltammetry (CV)

Cyclic voltammetry was carried out with a Gamry Reference 600 potentiostat in a three-electrode cell. The reference was an Ag/AgCl electrode (+0.199 V vs SHE, Radiometer Analytical) and the counter electrode was a graphitic rod. Solutions of 0.15 M H_2SO_4, 1 mM $Ru(NH_3)_6^{2+/3+}$ in 1 M KCl, 1 mM $Fe(CN)_6^{4-/3-}$ in 1 M KCl, 1 mM dopamine in PBS and 1 mM ascorbic acid in PBS were prepared to probe the electrochemical properties of the a-C films. H_2SO_4 and KCl were obtained from Merck, all other chemicals from Sigma-Aldrich. The pH of PBS was 7.4 and that of 0.15 M H_2SO_4 was 0.65. All CV and EIS measurements were repeated at least 3 times with different electrodes at room temperature. The solutions were purged with N_2

for at least 15 minutes and blanketed during measurements. Cyclic voltammagrams presented in the figures are individual but representative voltammograms of each a-C film.

3. Results and Discussion

3.1. TEM

The cross-sectional TEM micrographs of the reference and O14 films are shown in Figure 1. Both films exhibited an amorphous structure on top of the Si substrate. The O14 film seemed more homogeneous compared to the reference based on slight density changes appearing in the micrographs. Both films also exhibited areas 10-30 nm in diameter that had a slightly different orientation, although no crystallinity was observed. EDS analysis confirmed the presence of a thin SiO_x layer at the interface between Si and a-C. The SiO_x layer was approximately 1.9 nm thick for the reference (Fig. 1C) and 2.4 nm for O14 (Fig. 1D). It was also noted that the reference film was thicker than O14 (190 nm against 155 nm), which is explained by the lower deposition rate as the oxygen inflow increases as also reported by McKindra et al. [4].

3.2. HIM

The effect of oxygen incorporation on the surface morphology was investigated with helium-ion microscopy and pictures of the reference and O14 films are shown in Figure 2 A and B, respectively. The carbon films are very smooth with small features less than 50 nm in size. The feature size is slightly smaller, more rounded and the size distribution more uniform in O14 compared to ref. McKindra et al. also noticed a similar change in surface morphology of a-C films after addition of oxygen [4]. The observed surface features seem to correspond to the areas with a slightly different orientation seen on the TEM micrographs.

3.3. AFM

Surface roughness of the oxygenated films was studied by AFM. The AFM images are shown in Figure 3 and average roughness (R_a) values are gathered in Table 1. R_a of the reference was 1.69 nm and increasing oxygen inflow did not cause any significant changes. The highest value of 1.80 nm was observed for O10

and the lowest value of 1.59 nm for O14. The small and round features seen on the carbon films by AFM are consistent with surface morphology observed in the HIM pictures and TEM micrographs.

3.4. Raman spectroscopy

The Raman spectra of the oxygenated films (Fig. 4 A) exhibited a strong G peak arising from the bond stretching of pairs of sp^2-bonded C atoms in rings and olefinic chains. The D peak appeared as a shoulder of the G peak and is due to the breathing mode of aromatic rings in disordered carbon. The position of the G peak showed an increasing trend from 1561 cm^{-1} for the Ref to 1572 cm^{-1} for O14 (Fig. 4 B). At the same time, the I_D/I_G ratios varied between 2.51 and 2.76 without a clear trend (Fig. 4 B and Table 1). Based on the three-stage model to interpret visible Raman spectra of amorphous carbon proposed by Ferrari and Robertson [14], the oxygenated films may lie in stage 2 between nanocrystalline carbon (nc-C) and amorphous carbon (a-C). The absence of any crystalline areas in the TEM micrographs suggests that the carbon films are predominantly amorphous. The slight upward shift of the G peak could be related to bond ordering and/or clustering of the sp^2 phase towards nc-C as the oxygen content increases [14]. The shift towards stage 3, also associated with an increase in G peak position, can be excluded because the I_D/I_G ratio is close to 3 and increases in the end (O6-O14). Nonetheless, the changes in I_D/I_G and G peak position are quite small and it appears that the oxygen content in the studied range does not affect the carbon film structure significantly based on visible Raman. This could be explained by the fact that the oxygen content seemed to saturate in the bulk film above 6 sccm based on ToF-ERDA results (see section 3.6.). The oxygenated a-C films of McKindra et al. [4] showed a decreasing trend in I_D/I_G and similar G peak position with this study. The authors suggested that their films lie in stage 3 and the decreasing I_D/I_G could be due to graphitization when too much oxygen is added [4]. Santini et al.[5] also observed a decreasing I_D/I_G for increasing oxygen content in a-C films. G peak positions were not reported. The authors suggested based on Raman spectroscopy and XPS, that increasing O content leads to a decrease in the number of C sp^2 bonds and that the a-C film consists mostly of C-O groups bonded to a network of C-C sp^3 bonds with a small number of C-C sp^2 chains [5]. The oxygenated a-C films in these two studies were deposited by magnetron

sputtering and deposition parameters also differed in terms of plasma power and total working pressure so structural differences are expected compared to the films of this study.

3.5. XPS

The wide spectra (Fig. 5) showed a clear increase in O/C ratio from 0.09 to 0.19 with increasing oxygen inflow during deposition (Table 1). Accordingly, the percentage of C-C bonds decreased and that of C-O bonds increased. The high-resolution C 1s and O 1s spectra indicated that the number of carbon-oxygen bonds (C-O), ketone/aldehyde (C=O) and carboxyl-like (COO) groups steadily increased compared to the reference as the oxygen content rose in the films (Table 1). The oxygen in the films was uniformly distributed within the probing depth of XPS. All the a-C films contained small amounts of Fe (≤0.2 at. %) and N (≤0.7 at. %). Additionally, the reference and O2 films also contained small amounts of Ar (≤0.4 at. %).

3.6. ToF-ERDA

Histograms depicting time-of-flight versus energy and elemental depth profiles of the a-C films are shown in Figure 6. The elemental analysis from the bulk of the carbon films (Table 2) indicated that the reference film contains mostly carbon (85 at. %), some hydrogen (11 at. %) and oxygen (3.3 at. %), and small amounts of N, Fe, Cr and Ar impurities. Fe and Cr originated most likely from the stainless steel in the deposition chamber as trace amounts of Cr were also detected (not included in Table 2). These same impurities were also found in the oxygenated carbon films. In the reference film, oxygen exhibited a clear peak at the interface and a less pronounced one at the surface (Fig. 5A), indicating that oxygen was not as evenly distributed as in the oxygenated films.

In the oxygenated films, the concentration of oxygen seemed to plateau at about 11 at. % as increasing the O_2 inflow from 10 to 14 sccm did not result in a higher bulk concentration. The concentration of hydrogen also increased up to 17 at. % (O14) compared to 11 at. % for the reference. The oxygen had mostly a uniform distribution throughout the bulk of the oxygenated films consistent with XPS analysis. However, the oxygen was also more weakly bound, which was characterized by the bigger elemental loss during the measurements compared to the reference film. In addition, based on the number of

atoms per cm^2, it was noted that the reference film was thicker than the oxygenated films (as was measured from the cross-sectional TEM micrographs).

3.7. Conductive AFM

The average current (I) flowing through the oxygenated a-C films was obtained from c-AFM measurements and the results are shown in Table 1. A steady decrease in average current was observed from 6.52 to 0.11 nA as the oxygen content increased. This indicates that the resistivity of the a-C films increases significantly as more oxygen is incorporated, which was also reported previously by Santini et al. [5].

3.8. Electrochemical impedance spectroscopy

EIS measurements were carried out to characterize the electrochemical properties of the oxygenated a-C films. The Nyquist plots (Figure 7) were fitted to obtain the exponent *a*, solution resistance (R_s), charge transfer resistance (R_{ct}) and double layer capacitance (C_{dl}). The apparent heterogeneous electron transfer rate constant (k^0) was calculated using Equation 1. All the values are shown in Table 3.

The exponent *a* is a measure of the capacitive characteristics of the constant phase element used to describe C_{dl} and a value of 1 corresponds to an ideal capacitor. The obtained values were close to 1, thus indicating that all the a-C films behaved almost like ideal capacitors. R_s values were quite similar for all the films as well.

The R_{ct} values showed a clear division: the reference and lightly oxygenated films (O2 and O6) exhibited a low resistance around 50 Ω, whereas the highly oxygenated films (O10 and O14) had a considerably higher resistance around 7500 Ω. The increase in R_{ct} can be associated with the increase in resistivity seen by conductive AFM, since $Ru(NH_3)_6^{2+/3+}$ is an outer sphere redox probe and it is not influenced by surface properties of the electrodes. The drastic division in R_{ct} also coincides with the saturation of oxygen observed in the bulk of the film by ToF-ERDA. a-C films with an oxygen concentration of 3-9 at. % exhibit a low R_{ct} that increases by two orders of magnitude when the oxygen concentration reaches around 11 at. %. No

correlation could be made between R_{ct} and I_D/I_G, since the latter showed only slight variation and no clear trend as a function of oxygen content.

The slightly lower C_{dl} value of 0.98 ± 0.1 µF/cm^2 observed for the reference film compared to the oxygenated films (1.1 µF/cm^2) could be explained by the difference in amount of surface oxygen functional groups. The O/C ratio rose from 0.09 (Ref) to 0.13 (O2). However, further increase in O/C ratio from 0.13 (O2) to 0.19 (O14) did not increase double layer capacitance. The small differences in average surface roughness can also affect the C_{dl} values.

The fastest k^0 of 0.047 cm/s was obtained for the reference, closely followed by the lightly oxygenated a-C films with 0.028 cm/s (O2) and 0.033 cm/s (O6). The k^0 values decreased to 0.28 x 10^{-3} cm/s (O10) and 0.22 x 10^{-3} cm/s (O14) in accordance with the significant increase in R_{ct} observed for these heavily oxygenated films.

3.9. Cyclic voltammetry

Several redox systems were used to examine the electrochemical properties of the oxygenated a-C films including $Ru(NH_3)_6^{2+/3+}$, $Fe(CN)_6^{3-/4-}$, dopamine (DA) and ascorbic acid (AA). Among these redox systems, $Ru(NH_3)_6^{2+/3+}$ is the only one considered to be an outer sphere redox system whose electron transfer is insensitive to surface chemistry. The other redox systems, on the contrary, are inner sphere and their electron transfer is significantly affected by surface chemistry. Therefore, varying oxygen content at the surface of the a-C films may affect their electron transfer. The observed ΔE_p values for all the redox systems at 100 mV/s are summarized in Table 4.

The potential windows, shown in Figure 8, were determined in H_2SO_4. A threshold value of 400 µA/cm^2 was taken as the limit of the potential window in both anodic and cathodic directions. It can be seen from the CVs that the potential windows were roughly of the same size, from -1.2 V to +1.95 V, except for O14 (Table 4). A clear oxidation peak emerges around +0.6 V and becomes more evident as the amount of oxygen increases in the films. The same is observed for the cathodic peak around -0.5 V and explains the smaller potential

window for O14 especially in this region. In addition, the faradaic contribution to the capacitive current increased significantly with increasing oxygen content, since the C_{dl} values were almost identical for all the a-C films. This is explained by the increasing amount of surface oxygen functional groups that undergo redox reactions.

The cyclic voltammograms of $Ru(NH_3)_6^{2+/3+}$ (Fig. 9) showed that the electron transfer is reversible for the reference film. Lightly oxygenated a-C films (O2 and O6) also had a reversible ΔE_p that increased to 170 mV (O10) and further to 397 mV (O14) as the amount of oxygen increased. As mentioned previously, the electron transfer of $Ru(NH_3)_6^{2+/3+}$ is only affected by the electrical properties of the films and not the surface chemistry. As the oxygen content increases in the a-C films, the electron transfer becomes slower. XPS and ToF-ERDA results showed that the increase in oxygen content was practically uniform throughout the films without any evidence of formation of non-conducting, oxygen-rich surface layers that could hinder charge transfer. The increase in resistivity, R_{ct} and subsequently ΔE_p is therefore most likely cause by electron transport through the films (as opposed to electron transfer to the surface), which becomes significantly slower as the oxygen content inside the films increases.

For $Fe(CN)_6^{4-/3-}$, ΔE_p was significantly larger for the oxygenated films compared to the reference (Fig. 10). Interestingly, however, the more oxygenated O6 film had a smaller ΔE_p than the less oxygenated O2 film. O10 and O14 had considerably larger ΔE_p values than O2 and O6, but a clear trend in peak potential separation was not observed due to high standard deviation in ΔE_p. The increase in resistivity and subsequent changes in the R_{ct} values could explain the drastic increase in ΔE_p for the heavily oxidized films. However, in this case it should be noted that as $Fe(CN)_6^{4-/3-}$ is considered an inner sphere system, the changes in electrical properties may not solely explain differences in ΔE_p as the surface chemistry also significantly changes with oxygen addition. This is especially true for the lightly oxygenated films as the small changes in resistivity and R_{ct} cannot explain the clear increase in peak potential separation. Thus, it seems that oxygen functional groups also affect the electron transfer of $Fe(CN)_6^{4-/3-}$ to some degree.

Chen and McCreery have suggested that $Fe(CN)_6^{4-/3-}$ is surface sensitive, but that oxides should have only minor effects on its ΔE_p at GC electrodes [15]. However, our results indicate that $Fe(CN)_6^{4-/3-}$ is clearly affected by oxygen functional groups at the surface of the a-C films and similar observations have also been made in other studies. Surface oxygen functional groups have been shown to affect electron transfer of $Fe(CN)_6^{4-/3-}$ on reduced graphene oxide (rGO) [16] and basal and edge plane pyrolytic graphite (BPPG and EPPG, respectively) [17]. Tan et al. argued that increasing ΔE_p with increasing O/C ratio at rGO electrodes is explained by stronger electrostatic repulsion between dissociated oxygen groups and the negatively charged redox probe [16]. Ji et al. showed on BPPG and EPPG that oxygen functional groups formed by exposure to ambient air resulted in an increase in ΔE_p and decrease in heterogeneous electron transfer rate compared to similar, freshly prepared electrodes [17].

From the cyclic voltammograms of DA (Fig. 11 A), it can be seen that the ΔE_p values increased steadily from 124 mV (Ref) to 303 mV (O14). Thus, the reaction kinetics became more sluggish as the amount of oxygen increased in the a-C films. Dopamine is considered a surface sensitive redox system that requires adsorption to the surface to undergo oxidation [18], but it is not significantly affected by surface oxygen functionalities [9,18]. Instead, it has been suggested that DA oxidation is catalyzed by the presence of hydrogen bonding sites to facilitate proton-assisted electron transfer [9,19]. The amine group in DA is protonated in neutral pH giving it a positive charge [20] and therefore electrostatic repulsion between DA and the surface oxygen functional groups can be neglected. Compared to other highly sp^2-bonded nanocarbon films deposited by UBMS [7], the reference and lightly oxygenated films in this study show considerably faster kinetics for DA. This could be explained by higher surface roughness of the films in this study that may facilitate adsorption of DA. The increase in resistivity may also contribute to the increasing ΔE_p values for the highly oxygenated O10 and O14 films.

Since the oxidation of AA is totally irreversible and no reduction peak is observed on the cyclic voltammograms (Fig. 11 B), the oxidation peak potential (E_{pa}) values are compared instead of peak potential separation. As with DA, E_{pa} of AA increases with increasing oxygen content of the a-C films. AA has been classified as a surface sensitive redox probe, but its sensitivity to oxygen functional groups has been debated.

Chen and McCreery have shown that AA is insensitive to surface oxides on freshly prepared GC although longer exposure to air shifts the oxidation of AA [15]. Indeed, it has been shown that "pristine" carbon surfaces (void of impurities) [21], vacuum heat-treated GC (with fewer oxygen functional groups) [22] and edge-plane sites [23] have higher reactivity toward the oxidation of AA. On the other hand, oxygen plasma treatment and electrochemical oxidation of boron-doped diamond (BDD) greatly increase the oxidation potential of AA [24]. The authors suggested that the underlying cause is the increased amount of repulsive dipole-dipole moments between the oxidized BDD surface (and in particular carbonyl groups) and AA. From the XPS results, the amount of carboxyl and aldehyde/ketone groups (and their relative amount among C-O bonds) increased with the oxygen content in the a-C films, which could also explain the rising E_{pa} observed in this study. However, contribution of these specific groups is not unequivocal, since all the oxygen functional groups increased on the surface and the increase in resistivity observed for the heavily oxygenated films may also contribute to the increase in oxidation potential. Thus, this issue is not unambiguously resolved and further investigation (both experimental and computational) is required.

4. Conclusion

Amorphous carbon films with varying oxygen content were deposited by closed-field unbalanced magnetron sputtering. Their structure and surface chemistry was investigated and subsequently correlated with their electrochemical properties. TEM micrographs and Raman spectroscopy confirmed that the films are amorphous with I_D/I_G ratios around 2.6. The ToF-ERDA analysis showed that the oxygen content in the bulk of the films seems to saturate at around 11 at. %, since no increase in oxygen content was observed with higher inflow during deposition. The amount of surface oxygen functional groups, however, increased steadily and O/C ratio increased from 0.09 to 0.19. The conductive AFM results showed that the resistivity of the a-C films significantly increased with oxygen incorporation.

Lightly oxygenated a-C films (ref, O2, O6) exhibited low charge transfer resistances that increased by two orders of magnitude for the heavily oxygenated films (O10, O14) that had reached oxygen saturation in the bulk film. Double layer capacitance values were not significantly affected by the oxygen content and were around 1 $\mu F/cm^2$.

Lightly oxygenated a-C films showed reversible electron transfer in $Ru(NH_3)_6^{2+/3+}$ but ΔE_p increased considerably for heavily oxygenated films according to the increase in film resistivity. The inner sphere redox systems were significantly affected, not only by the changes in the film resistivity, but also by the surface oxygen functional groups. ΔE_p increased linearly with the increase in oxygen content for the oxidation of DA, and similarly E_{pa} increased for the oxidation of AA. $Fe(CN)_6^{3-/4-}$ did not show a clear trend but was still clearly affected by the surface oxygen functional groups

Acknowledgements

T.P. and T.L. acknowledge the financial support from the Academy of Finland (grant numbers #285015 and #285526). The authors also acknowledge the provision of facilities at the Nanomicroscopy Center and Micronova Nanofabrication Center by Aalto University. T.P. acknowledges Ms. Elli Leppänen for help with the CV measurements.

References

[1] S.I. Kim, B.B. Sahu, B.M. Weon, J.G. Han, J. Koskinen, S. Franssila, Making porous conductive carbon films with unbalanced magnetron sputtering, Jpn. J. Appl. Phys. 54 (2015) 010304.

[2] S.I. Kim, B.B. Sahu, S.E. Kim, A. Ali, E.H. Choi, J.G. Han, Controlling conductivity of carbon film for L-929 cell biocompatibility using magnetron sputtering plasmas, J. Mater. Chem. B 3 (2015) 3267-3278.

[3] T. Kamata, D. Kato, S. Umemura, O. Niwa, Structure and Electroanalytical Application of Nitrogen-doped Carbon Thin Film Electrode with Lower Nitrogen Concentration, Anal. Sci. 31 (2015) 651-656.

[4] T. McKindra, M.J. O'Keefe, R. Cortez, Reactive sputter-deposition of oxygenated amorphous carbon thin films in Ar/O2, Diam. Relat. Mater. 20 (2011) 509-515.

[5] C.A. Santini, A. Sebastian, C. Marchiori, V.P. Jonnalagadda, L. Dellmann, W.W. Koelmans, et al., Oxygenated amorphous carbon for resistive memory applications, Nat. Commun. 6 (2015).

[6] E. Kaivosoja, S. Sainio, J. Lyytinen, T. Palomäki, T. Laurila, S.I. Kim, et al., Carbon thin films as electrode material in neural sensing, Surf. Coat. Technol. 259, Part A (2014) 33-38.

[7] T. Kamata, D. Kato, H. Ida, O. Niwa, Structure and electrochemical characterization of carbon films formed by unbalanced magnetron (UBM) sputtering method, Diam. Relat. Mater. 49 (2014) 25-32.

[8] H. Yanagisawa, R. Kurita, T. Kamata, K. Yoshioka, D. Kato, A. Iwasawa, et al., Effect of the sp^2/sp^3 Ratio in a Hybrid Nanocarbon Thin Film Electrode for Anodic Stripping Voltammetry Fabricated by Unbalanced Magnetron Sputtering Equipment, Anal. Sci. 31 (2015) 635-641.

[9] R.L. McCreery, Advanced Carbon Electrode Materials for Molecular Electrochemistry, Chem. Rev. 108 (2008) 2646-2687.

[10] L. Johansson, J.M. Campbell, Reproducible XPS on biopolymers: cellulose studies, Surf. Interface Anal. 36 (2004) 1018-1022.

[11] G. Beamson, D. Briggs, High resolution XPS of organic polymers, Wiley 1992.

[12] M. Laitinen, M. Rossi, J. Julin, T. Sajavaara, Time-of-flight – Energy spectrometer for elemental depth profiling – Jyväskylä design, Nucl. Instrum. Methods Phys. Res. , Sect. B 337 (2014) 55-61.

[13] K. Arstila, J. Julin, M.I. Laitinen, J. Aalto, T. Konu, S. Kärkkäinen, et al., Potku – New analysis software for heavy ion elastic recoil detection analysis, Nucl. Instrum. Methods Phys. Res. , Sect. B 331 (2014) 34-41.

[14] A.C. Ferrari, J. Robertson, Interpretation of Raman spectra of disordered and amorphous carbon, Phys. Rev. B 61 (2000) 14095-14107.

[15] P. Chen, R.L. McCreery, Control of Electron Transfer Kinetics at Glassy Carbon Electrodes by Specific Surface Modification, Anal. Chem. 68 (1996) 3958-3965.

[16] S.M. Tan, A. Ambrosi, C.K. Chua, M. Pumera, Electron transfer properties of chemically reduced graphene materials with different oxygen contents, J. Mater. Chem. A 10668.

[17] X. Ji, C.E. Banks, A. Crossley, R.G. Compton, Oxygenated Edge Plane Sites Slow the Electron Transfer of the Ferro-/Ferricyanide Redox Couple at Graphite Electrodes, ChemPhysChem 7 (2006) 1337-1344.

[18] S.H. DuVall, R.L. McCreery, Control of Catechol and Hydroquinone Electron-Transfer Kinetics on Native and Modified Glassy Carbon Electrodes, Anal. Chem. 71 (1999) 4594-4602.

[19] S.H. DuVall, R.L. McCreery, Self-catalysis by Catechols and Quinones during Heterogeneous Electron Transfer at Carbon Electrodes, J. Am. Chem. Soc. 122 (2000) 6759-6764.

[20] T. Palomäki, S. Chumillas, S. Sainio, V. Protopopova, M. Kauppila, J. Koskinen, et al., Electrochemical reactions of catechol, methylcatechol and dopamine at tetrahedral amorphous carbon (ta-C) thin film electrodes, Diam. Relat. Mater. 59 (2015) 30-39.

[21] I.F. Hu, T. Kuwana, Oxidative mechanism of ascorbic acid at glassy carbon electrodes, Anal. Chem. 58 (1986) 3235-3239.

[22] D.T. Fagan, I.F. Hu, T. Kuwana, Vacuum heat-treatment for activation of glassy carbon electrodes, Anal. Chem. 57 (1985) 2759-2763.

[23] F. Wantz, C.E. Banks, R.G. Compton, Direct Oxidation of Ascorbic Acid at an Edge Plane Pyrolytic Graphite Electrode: A Comparison of the Electroanalytical Response with Other Carbon Electrodes, Electroanal. 17 (2005) 1529-1533.

[24] H. Notsu, I. Yagi, T. Tatsuma, D.A. Tryk, A. Fujishima, Introduction of Oxygen-Containing Functional Groups onto Diamond Electrode Surfaces by Oxygen Plasma and Anodic Polarization, Electrochem. Solid-State Lett. 2 (1999) 522-524.

Tables:

Table 1. Characterization data: oxygen inflow during deposition, I_D/I_G ratio, average surface roughness (R_a), average current through the films (I) and XPS results for the a-C films.

Sample	O_2 (sccm)	Raman	AFM	c-AFM	XPS			
		I_D/I_G	R_a (nm)	I (nA)	O/C	C-C (%)	C-O (%)	C=O (%)	COO (%)
Ref	0	2.62 ± 0.02	1.69 ± 0.09	6.52 ± 3.0	0.09	79.4	13.6	4.1	2.9
O2	2	2.76 ± 0.07	1.78 ± 0.07	1.24 ± 0.6	0.13	75.9	15.2	5.3	3.5
O6	6	2.49 ± 0.02	1.65 ± 0.04	0.67 ± 0.4	0.16	73.5	16.4	6.2	3.9
O10	10	2.51 ± 0.08	1.80 ± 0.06	0.42 ± 0.1	0.18	71.2	17.6	7.0	4.2
O14	14	2.67 ± 0.06	1.59 ± 0.03	0.11 ± 0.0	0.19	69.8	18.4	7.2	4.6

Table 2. Concentrations from the depth profiles of the a-C films measured by ToF-ERDA (O2 was not measured).

Sample	Concentration ± error (at. %)					
	H	C	N	O	Fe	Ar
Ref	11 ± 1.5	85 ± 2.0	0.3 ± 0.1	3.3 ± 0.3	0.9 ± 0.2	0.4 ± 0.1
O6	14 ± 1.5	76 ± 2.0	0.5 ± 0.1	9 ± 1.0	0.5 ± 0.2	0.06 ± 0.0
O10	15 ± 1.5	73 ± 2.0	0.8 ± 0.2	11 ± 1.0	0.4 ± 0.2	0.03 ± 0.0
O14	17 ± 1.5	70 ± 2.0	1.0 ± 0.2	11 ± 1.0	0.6 ± 0.2	0.04 ± 0.0

Table 3. Parameters obtained by fitting the Nyquist plots with the Randles circuit model described in section 2.8.. k^0 was calculated using equation (1).

Sample	*a*	R_s (Ω)	R_{ct} (Ω)	C_{dl} (μF/cm^2)	k^0 (cm/s)
Ref	0.95 ± 0.0	24 ± 8.4	44 ± 21	0.98 ± 0.1	0.047 ± 0.0
O2	0.99 ± 0.0	15 ± 0.6	55 ± 4.3	1.1 ± 0.0	0.028 ± 0.0
O6	0.99 ± 0.0	16 ± 0.6	50 ± 14	1.1 ± 0.0	0.033 ± 0.0
O10	0.97 ± 0.0	16 ± 0.3	7540 ± 4530	1.1 ± 0.1	(0.28 ± 0.15) x 10^{-3}
O14	0.97 ± 0.0	45 ± 45	7470 ± 2620	1.1 ± 0.0	(0.22 ± 0.10) x 10^{-3}

Table 4. Potential windows and observed ΔE_p for 1 mM $Ru(NH_3)_6^{3+/2+}$ in 1 M KCl, 1 mM $Fe(CN)_6^{4-/3-}$ in 1 M KCl, 100 μM dopamine in PBS and E_{pa} for 1 mM ascorbic acid in PBS. Scan rate was 100 mV/s. The values are averages from 3 different samples.

Sample	Potential window (V)	ΔE_p (mV) ± STD (N = 3)			E_{pa} (mV) ± STD (N = 3)
		$Ru(NH_3)_6^{3+/2+}$	$Fe(CN)_6^{4-/3-}$	DA	AA
Ref	3.17	59.8 ± 0.0	139 ± 12	124 ±18	390 ± 30
O2	3.21	62.8 ± 0.8	306 ± 51	159 ± 9.0	443 ± 34
O6	3.11	61.5 ± 1.2	235 ± 14	198 ± 19	500 ± 42

O10	3.18	170 ± 20	646 ± 38	238 ± 11	618 ± 25
O14	2.91	397 ± 47	599 ± 84	303 ± 23	725 ± 28

Figure captions:

Figure 1. Cross-sectional TEM micrographs of A) and C) Ref, and B) and D) O14. Micrographs in A) and B) were taken from the bulk of the films whereas C) and D) show the interface with the Si substrate at the bottom.

Figure 2. HIM pictures showing the surface morphology of the A) Ref and B) O14 a-C films. The size of the pictures is 1 µm x 1 µm.

Figure 3. AFM images of the surface of the A) Ref, B) O2, C) O6, D) O10 and E) O14 a-C films. The size of the scanned area was 2 µm x 2 µm.

Figure 4. Raman measurements of the oxygenated carbon films. A) Raman spectra and B) I_D/I_G ratio and G peak position as a function of oxygen inflow during deposition.

Figure 5. XPS wide spectra of the reference and oxygenated a-C films.

Figure 6. A) Histogram depicting time-of-flight versus energy and B) corresponding depth profile of the reference film. C) and D) present the respective information for the O6 film for comparison. Elemental compositions normalized to 100 % for all depths. In A) and B) the clear continuation of Si up to the surface is most likely caused by a tiny crack in the film at the measurement position.

Figure 7. A) Nyquist plots of the a-C films obtained from EIS measurements in 5 mM $Ru(NH_3)_6^{2+/3+}$. B) Inset of the high frequency region where Ref, O2 and O6 are easily seen.

Figure 8. Potential windows of the a-C films in 0.15 M H_2SO_4. Scan rate 100 mV/s.

Figure 9. Cyclic voltammograms of the a-C films in 1 mM $Ru(NH_3)_6^{2+/3+}$ in 1 M KCl. Scan rate 100 mV/s.

Figure 10. Cyclic voltammograms of the a-C films in 1 mM $Fe(CN)_6^{4-/3-}$ in 1 M KCl Scan rate 100 mV/s.

Figure 11. Cyclic voltammograms in A) 100 µM dopamine and B) 1 mM ascorbic acid in PBS at the a-C films. Scan rate 100 mV/s.